Dynamic Interference Analysis of Coexisting Mobile WBANs for Health Monitoring

Xiaoming Yuan[1], Changle Li[1*], Kuan Zhang[2], Qiang Ye[3], Nan Cheng[3], Ning Zhang[4], and Xuemin (Sherman) Shen[3]
[1]State Key Laboratory of Integrated Services Networks, Xidian University, Xi'an, Shaanxi 710071, China
[2]Department of Electrical and Computer Engineering, University of Nebraska-Lincoln, Omaha, NE 68182, USA
[3]Department of Electrical and Computer Engineering, University of Waterloo, Waterloo, ON N2L 3G1, Canada
[4]Department of Computing Sciences, Texas A&M University-Corpus Christi, Corpus Christi, TX 78412, USA
[*]E-mail: clli@mail.xidian.edu.cn

***Abstract*—Wireless Body Area Network (WBAN) technology jumps into popularity owing to its real-time ability and high reliability in health monitoring. The accompanying interference problem must be highly concerned in coexisting densely deployed WBANs since the inter-WBAN interference results in high delay and low reliability data transmissions, especially with the movement of human body. In the paper, we analyze the dynamic interference with human mobility in multiple coexisting WBANs with the consideration of different distances between inter-WBANs and varying number of coexisting WBANs. Moreover, we investigate the influence of inter-WBAN interference on the performance of normalized throughput and average access delay of different traffic types. The results show that the interference generated by mobile neighbour WBANs extremely decreases the throughput of the target WBAN and increases the average packet delay 1.76 times of emergency data compared with the target WBAN without interference. The dynamic interference analysis provides insights on the practical WBAN management and interference mitigation protocol design, especially for the deeply deployed coexisting WBAN scenarios.**

I. Introduction

Wireless Body Area Networks (WBANs) are highly reliable wireless communication networks and can effectively provide real-time and continuous painstaking care for health monitoring in e-healthcare. A WBAN consists of several sensors interconnected on the surface, inside, or in the proximity of the human body that communicate their readings back to a hub device on or near the individual [1] [2]. With the flexibility, scalability and low-cost characteristics, WBANs have become one of the primary technologies for the ubiquitous Internet-of-Things (IoTs) [3] [4] to enhance the quality of people's life.

Inter-WBAN interference is generated by two or more adjacent WBANs transmitting data simultaneously in dense WBANs application scenarios, such as wards and waiting rooms in hospitals and public transports. The interference of coexisting deeply employed WBANs deteriorates the reliability and timeliness of data transmissions and increases network management cost [5], which could threaten the life safety of human in health diagnosis and increase the economic cost paid on healthcare. The inter-WBAN interference problem in adjacent WBANs has been addressed in [6]. The inter-WBAN coexistence and interference mitigation schemes are surveyed and discussed in [7]. Xuan et al. [8] focused on the interference analysis for co-channel interference of non-overlapping WBANs scenario. Wen et al. [9] analyzed the interuser interference in IEEE 802.15.6 based WBANs and derived the optimal interference detection range to tradeoff between outage probability and spatial throughput.

However, few attention has been paid to the interference dynamics of inter-WBANs caused by human mobility. Inter-WBAN interference is in dynamic variation due to the inherent mobility of human and the human-centric characteristics of WBANs. The topology of WBANs is changing with the human movement, which leads to the inter-WBAN interference varying with the relative location of the target WBAN and adjacent WBANs. Zhang et al. modeled the inter-WBANs interference in an non-overlapping WBAN topology and calculated the cumulative distribution function of the interference distances [10] while Cheng et al. [11] employed a cylinder model to perform the interference detection. Whereas, the dynamic topology of WBANs should be paid more attention. Interference could last for a short time when someone just passes by or for a relative long period when friends or patients remain close for several hours. The effects of passerby movement types were analyzed and compared to the effects of users motions such as walking and running [12]. The network performance on throughput and delay change with the variable interference and become severe when adjacent WBANs are deeply overlapped with each other. Therefore, analyzing the dynamic interference in coexisting multi-WBANs is required, which satisfies the practical scenario well and can greatly benefit interference mitigation as well as network design, management and optimization for WBANs.

In this paper, we analyze the interference of coexisting WBANs by considering the human mobility. The movement of neighbouring WBANs in rectilinear motion and curvilinear motion cases are investigated. The interference dynamics in different situations such as different distances between inter-WBANs and varying number of coexisting overlapped W-BANs are taken into account. Meantime, the asynchronous Carrier Sense Multiple Access with Collision Avoidance (CSMA/CA)-based IEEE 802.15.6 Medium Access Control (MAC) mechanism [13] is developed to improve the scalability

978-1-5386-3180-5/18/$31.00 ©2018 IEEE

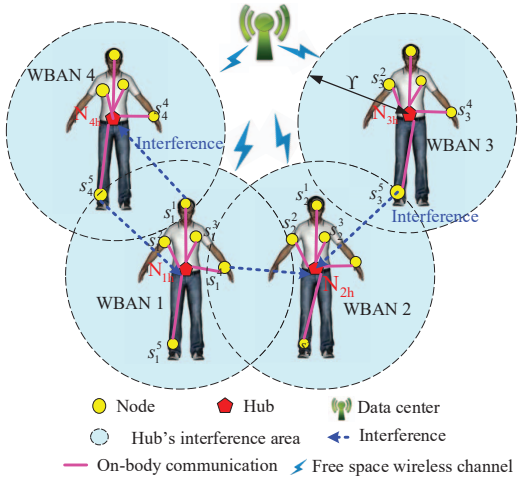

Fig. 1: Network model.

of a WBAN. The normalized throughput and average access delay of different User Priorities (UP) are investigated under the impact of dynamic interference from neighboring WBANs.

The remainder of paper is organized as follows. The system model is presented in Section II. In Section III, the interference dynamics are described. Performance on normalized throughput and average packet access delay are analyzed in Section IV. Section V demonstrates analytical results and discussions. Section VI concludes the paper and highlights our future work..

II. SYSTEM MODEL

There is a set of coexisting WBANs $\{N_m|m = 1, 2, \ldots, M\}$ in the system, where M is the number of WBANs and N_m stands for WBAN m, as shown as in Fig. 1. The hub is denoted by $\{N_{mh}|m = 1, 2, \ldots, M\}$ and several numbered physiological sensor nodes are denoted by $\{s_m^y|y = 1, 2, \ldots, Y\}$. Only one-hop topology of a WBAN is considered. The Hub is usually performed by a smartphone or a personal digital assistant (PDA), which has greater power and computing capability with power-rechargeable. The collected data traffic is transmitted from nodes to the hub through on-body channel in IEEE 802.15.6-based CSMA/CA and transmitted from hub to the center controller in free space wireless channel. The channel conditions are considered ideal during the data transmission.

The sensing health data should be classified into different data or user priorities to satisfy the diversified performance requirements. In IEEE 802.15.6, eight user priorities $(UP_k, k = 0, 1, 2, ..., 7)$ are predefined [13]. The higher user priority has privilege to access the channel. The user priorities of medical data traffic are from 5 to 7 generally, guaranteeing the severer traffic in high priority to be transmitted timely.

We consider that the interference range of sensor nodes is Υ and define the distance between N_1 and N_m as the distance from N_{1h} to N_{mh}. With the movement of human body, the distance between WBANs is constantly changing. There is no interference between WBANs such as N_3 and N_4. The

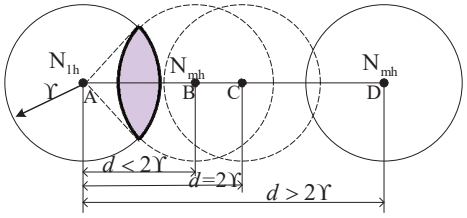

Fig. 2: The relative position of N_1 and N_m.

interference occurs between the adjacent WBANs if there are senor nodes in the communication area of neighbor WBANs, as the distribution of N_1, N_2 and N_3 illustrated in Fig. 1. Information transmission of s_3^5 in N_3 increases the collision probability of data transactions in N_2. As the inter-WBANs distances decrease, the communication zones are overlapped partially. The mutual interference problem aggravates the performance of the network in the overlapped area. The data transmissions of sensor node s_1^4 in the overlapped area of N_1 and N_2 can directly intrude all the data transactions of N_2. Since the distance between s_1^4 and N_{2h} is less than the interference range Υ that s_1^4 disturbs the data transactions of hub N_{2h}. If the distance of N_1 and N_2 becomes smaller, the overlapped area as well as the number of interference nodes increases. The worst case is two or more communication zones are completely overlapping, and the performance of all the WBANs in the system are serious.

III. DYNAMIC INTERFERENCE OF COEXISTING MOBILE WBANS

In the public area of nursing homes or hospitals, each patient carries a mobile WBAN with several sensor nodes attached on their body to monitor their health data. The interference will generate if any two of the patients are too close to each other. In this section, we calculate the changing interfering nodes and discuss the dynamic interference of multiple coexisting WBANs in different cases.

A. The Calculation of Interfering nodes

The mutual interference of multi-WBAN coexistence is caused by the data transactions of sensor nodes from neighbor WBANs. We assume all the WBANs in same configuration. The topology of a WBAN can be modeled as a circle centered at the hub. The hub is located near the center of a human body with the communication range Υ. The projection of all the nodes is relative uniformly random distribution within the circle. The modeled topology of a WBAN is two dimensional for the tractable analysis instead of the three-dimensional distribution in reality.

The interference intensity is directly related to the relative location and the number of jamming nodes. Assuming N_1 as the target WBAN, we firstly pay our attention to the affection of one existing random neighbour WBAN N_m. Every hub knows its coordinate in the network. The coordinates of N_{1h} and N_{mh} are (x_{1h}, y_{1h}) and (x_{mh}, y_{mh}), respectively. As stated earlier in the system model, the distance d between N_1

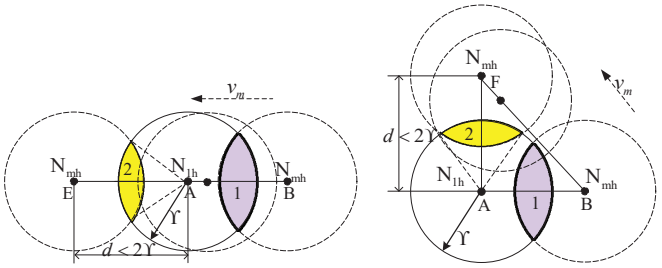

(a) Rectilinear motion

(b) Redirection curvilinear motion

Fig. 3: The relative motion of N_m.

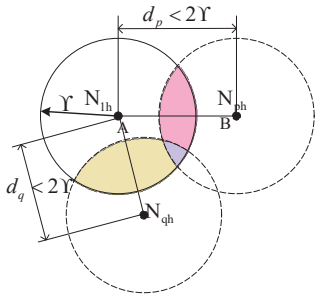

Fig. 4: The relative position of three WBANs.

and N_m is the distance from N_{1h} to N_{mh}. Hence the distance d can be calculated as

$$d = \sqrt{(x_{mh} - x_{1h})^2 + (y_{mh} - y_{1h})^2} \tag{1}$$

An arbitrary WBAN N_m moves in the direction of target WBAN N_1, there are three relative positions of the two WBANs, as shown in Fig. 2. If $d > 2\Upsilon$, there is no inference between them. N_m keeps moving from position D to position C, then it reaches the edge that can interfere N_1. We mark this critical point when $d = 2\Upsilon$ as the moment $t = 0$. Supposing that N_m continue moving to N_1 till position B where d is less than 2Υ resulting in an overlap of the communication zones. Sensor nodes of N_m in the overlapped area become interference sources, increasing the collision probability of data transactions of the tagged WBAN and decreasing the network performance on throughput and packet delay meanwhile. The number of interference nodes n_I can be calculated as Eq. (2) at this case.

$$n_I = \frac{2Y}{\pi\Upsilon^2} \times \left(\arccos\frac{d}{2\Upsilon}\Upsilon^2 - \frac{d}{2}\sqrt{\Upsilon^2 - \frac{d^2}{4}} \right) \tag{2}$$

where Y is the number of sensor nodes in a WBAN. The relative position of N_m and the tagged WBAN N_1 is perhaps maintained the present status for a period of time. The maximum number of interfering nodes can be reached at $d = 0$ where the two WBANs are totally overlapped, the value of which is Y. The interference nodes continuously affect the performance of N_1 until N_m leaves.

The moving direction of N_m at next moment is uncertain since people have a variety of options. In general, the movement of N_m could be classified in two cases: rectilinear motion and curvilinear motion. The rectilinear motion of N_m means that it leaves in original direction or the opposite. The angle between the leaving velocity vector and the approaching velocity vector is zero or π, as shown in Fig. 3(a). N_{mh} moves from position B to position E. Section 1 is the original overlapping area while section 2 is the overlapping area at the next moment. The curvilinear motion refers that the angel between the leaving velocity vector and the approaching velocity vector takes values in an interval (0,π). One kind of leaving motion is shown in Fig. 3(b). N_mh moves from position B to position F. The number of interference nodes is decided by the relative position of the WBANs, i.e., the overlapping area. The Eq. (2) is applicable for both of the two cases to calculate the number of interfering nodes. The velocity of N_{mh} is denoted by v_m, which direction affects the duration of the interference. The interference in rectilinear motion sustains a little longer than that in curvilinear motion.

B. Multiple Coexisting Mobile WBANs

For the coexistence of more than two WBANs, the distance between any WBAN and the tagged WBAN determines the number of interference nodes. It makes no great difference to the tagged WBAN whether the other WBANs have overlap or not. In other words, we only focus on the number of nodes in the interference range of tagged WBAN and ignore the interference among any other WBANs. One case that any two of the three WBANs have an overlap is described in Fig. 4. The number of nodes in the intersection of N_p and N_q will not change the number of interfering nodes of N_p and N_q in the interference range of N_1. The number of interference nodes in the tagged WBAN N_1 can be obtained using Eq. (3).

$$\begin{aligned} n_I = {} & \tfrac{2Y}{\pi}\left(\arccos\tfrac{d_p}{2\Upsilon} + \arccos\tfrac{d_q}{2\Upsilon}\right) - \\ & \tfrac{Y}{\pi\Upsilon^2}\left(d_p\sqrt{\Upsilon^2 - \tfrac{d_p^2}{4}} + d_q\sqrt{\Upsilon^2 - \tfrac{d_q^2}{4}}\right) \end{aligned} \tag{3}$$

where $d_p = \sqrt{(x_{ph} - x_{1h})^2 + (y_{ph} - y_{1h})^2}$ and $d_q = \sqrt{(x_{qh} - x_{1h})^2 + (y_{qh} - y_{1h})^2}$, respectively.

Given that the high density of M concurrent WBANs at the same place, it is necessary to estimate the number of interfering WBANs since the interfering WBANs can increase collisions and data loss at the target WBAN. The interference from the other WBANs to the tagged WBAN depends on their distance. Therefore, the potential interference sources sets to the target WBAN at moment t could be represented as $\{N_K \,|0 \le K \le M; \forall K,\ d_k < 2\Upsilon\}$. The total number of interference nodes is

$$n_I = \frac{2Y}{\pi\Upsilon^2} \sum_{m \in K} \left(\arccos\frac{d_m}{2\Upsilon}\Upsilon^2 - \frac{d_m}{2}\sqrt{\Upsilon^2 - \frac{d_m^2}{4}} \right) \tag{4}$$

where d_m is the distance from a WBAN in the interference source sets to the target WBAN.

IV. PERFORMANCE ANALYSIS

Multiple concurrent WBANs share the same operating channel. Sensors in different WBANs may collide over the channels. The arrival traffic of other WBANs interferes the current transmission, increasing the collision probability and average packet delay. In this section, we analyzed the performance analysis on normalized throughput and average packet delay of different user priorities.

We suppose that there are M WBANs in a dense deployment scenario at the same time. There are one hub and n_k nodes of UP_k, where $\sum_{k=0}^{7} n_k = Y, k = 0, ..., 7$, operates in the beacon mode with superframe boundaries in a random selected target WBAN. Assuming that the access probability of node UP_k in a random CSMA/CA slot is τ_k. The access probability of interference nodes is considered sharing the same probability with a UP_k node. The probability that channel is idle P_{idle} during the contention intervals of the target WBAN is

$$P_{idle} = \prod_{k=0}^{7} (1 - \tau_k)^{n_k} \tag{5}$$

There are n_I interference sources affecting the data transactions. Supposing that the node finds the channel is idle in probability P_{kidle} during its backoff period, the P_{kidle} is described as

$$\begin{aligned} P_{kidle} = & \frac{(1-\tau_k)^{n_I+n_k} \prod_{i \neq k} (1-\tau_i)^{n_i}}{(1-\tau_k)} \\ = & (1-\tau_k)^{n_I-1} \prod_{i=0}^{7} (1-\tau_k)^{n_k} \end{aligned} \tag{6}$$

The packet collision probability for each UP_k node at any backoff stage equals the probability of busy channel P_b and could be expressed as

$$P_b = 1 - P_{kidle} = 1 - (1-\tau_k)^{n_I-1} \prod_{i=0}^{7} (1-\tau_k)^{n_k} \tag{7}$$

We define the normalized throughput as the ratio of time cost of average successful transmitted payloads to the total intervals between two consecutive transmissions. A successful packet transmission time is T_{pk} and can be obtained from

$$\begin{aligned} T_{\mathrm{pk}} &= \frac{N_{packet}}{R_s} \\ &= \frac{N_{preamble} + N_{header} \times S_{header} + \frac{N_{total} \times S_{PSDU}}{\log_2 M}}{R_s} \end{aligned} \tag{8}$$

where R_s is the sysmbol rate. $N_{preamble}$ and N_{header} stand for the length of Physical Layer Convergence Protocol (PLCP) preamble and header, respectively. S_{header} denotes the spreading factor for the PLCP header. S_{PSDU} denotes the spreading factor for Physical Service Data Unit (PSDU). M is the cardinality of the constellation of a given modulation scheme. N_{total} is the total bits which flow in the PHY layer and can be derived in Eq. 9.

$$\begin{aligned} N_{total} = N_{PSDU} + \log_2 M \left\lceil \frac{N_{PSDU} + (n-k)N_{CW}}{\log_2 M} \right\rceil \\ + (n-k)N_{CW} - [N_{PSDU} + (n-k)N_{CW}] \end{aligned} \tag{9}$$

where N_{CW} denotes the number of Bose, Ray-Chaudhuri, Hocquenghem code (BCH) codewords in a frame. In IEEE 802.15.6, $N_{CW} = \lceil \frac{N_{PSDU}}{k} \rceil$, where n and k are selected by BCH encoder to achieve the desired code rate k/n. N_{PSDU} is the length of the PSDU. This component is formed by concatenating the MAC header with the MAC payload and frame check sequence (FCS). Given the length of MAC header $N_{MHeader}$, MAC payload $N_{MPayload}$ and FCS N_{FCS}, the N_{PSDU} can be acquired from Eq. (10).

$$N_{PSDU} = 8 \times (N_{MHeader} + N_{MPayload} + N_{FCS}) \tag{10}$$

$$T_{MPayload} = \frac{N_{MPayload} \times S_{PSDU}}{\log_2 M \times R_s} \tag{11}$$

The normalized throughput is

$$S_k = \frac{\tau_k P_{kidle} T_{MPayload}}{P_{idle} T_{c-slot} + \tau_k P_{kidle} T_{pk} + \tau_k (1 - P_{kidle}) T_{fpk}} \tag{12}$$

where T_{c-slot} is the contended CSMA/CA slot length. The length of an allocation slot T_{slot} is equal to $pAllocationSlotMin + L \times pAllocationSlotResolution$. P_{kidle} is the probability that the channel is idle during the backoff period of node UP_k. T_s in Eq. (13) is the mean time of a successful transmission.

$$T_s = T_{pk} + T_{pSIFS} + T_{I-ACK} \tag{13}$$

While the occupied slot length for a failure packet delivery T_{fpk} is described as

$$T_{fpk} = T_{pk} + T_{pSIFS} + T_{timeout} \tag{14}$$

A unreceived I-ACK in an interval $T_{timeout}$ will be treated as failure transmission. The T_{fail} is the total time cost before a packet has been successful transmitted.

$$T_{fail} = \sum_{l=0}^{BT_{\max}} l P_b{}^l (T_{pk} + T_{pSIFS} + T_{timeout}) + T_{kCW} \tag{15}$$

where l is the failure times before the packet is successfully transmitted. T_{kCW} is the backoff time in CSMA/CA and can be calculated in Eq. 16 [14]. B_{max} is the maximum backoff times. $CW_{\min[UP_k]}$ and $CW_{\max[UP_k]}$ is the contention window value boundaries of different user priorities and can be refered in [13].

$$T_{kCW} = \sum_{l=0}^{B_{max}} \frac{T_{c-slot} \left(CW_{\min[UP_k]} + CW_{\max[UP_k]} \right)}{4} \tag{16}$$

The average packet delay is defined as the time interval from the packet is ready to be transmitted to the moment the I-ACK

TABLE I: System parameters

Parameters	Value	Parameters	Value
Superframe length	1 s	FCS	2 bytes
CSMA slot length	145 μs	Coderate(k/n)	51/63
pAllocationSlotMin	500 μs	L	7
pAllocationResolution	500μs	M	4
MAC header	7 bytes	S_{header}	4
PLCP preamble	90 bits	S_{PSDU}	1
PLCP header	31 bits	pCCA time	105 μs
Symbol rate	600 ksps	pSIFS	75 μs
Frequency band	2400-2438.5 MHz	Timeout	30 μs

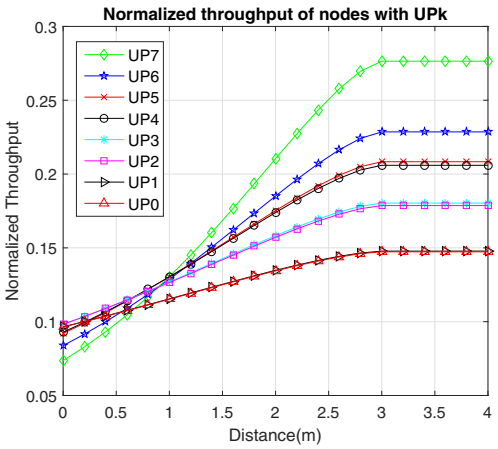

Fig. 5: Normalized throughput versus the distance between N_1 and N_m.

frame of this packet is received. In Eq. (17), the average delay D_k is given as

$$D_k{=}T_s + T_{fail} \tag{17}$$

By substituting Eqs. (13) and (15) into Eq. (17), the average access delay can be calculated. Both the normalized throughput and the average access delay consider the traffic differentiation and interference dynamics in the analysis.

V. PERFORMANCE EVALUATION

In this section, we evaluate the normalized throughput and the average access delay of coexisting IEEE 802.15.6-based WBANs. There are 8 nodes with payload of 100 bytes in this scenario. We consider each node in the WBAN only collect one kind of physiological data and the WBAN is saturated that every node in the network always has packets to contend the channel. The communication coverage radius of N_1 is 1.5 m. The other relevant parameters used are listed in Table I.

A. Normalized Throughput

We investigate how the distance between the target WBAN N_1 and a random WBAN N_m effect the performance on normalized throughput of the nodes with user priorities varying from 0 to 7 in Fig. 5. The interference intensity is the largest when the relative distance between N_1 and N_m is zero. The performance of the network is the worst, especially the UP7

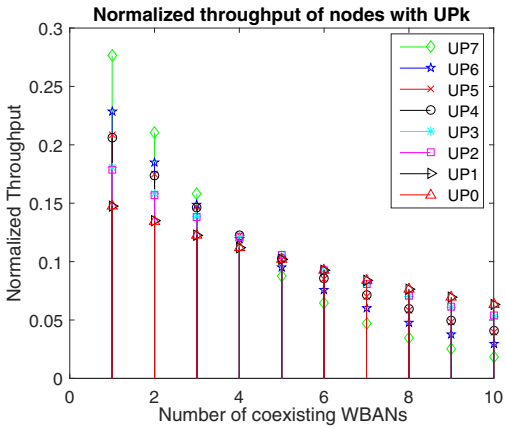

Fig. 6: Normalized throughput versus the number of coexisting WBANs.

node. When the distance changes from 0 to 3 m, the growth of normalized throughput is 0.203, 0.145, 0.116, 0.082 and 0.051 for UP_7, UP_6, UP_5, UP_3 and UP_1 node respectively. The variation of high UPs is larger than that of low UPs. Since the higher the user priority is, the higher collision probability is to access the channel. As the WBAN N_m moves far away from N_1, the number of interfering nodes decreases and the collisions between nodes reduce, then more data packets can be transmitted successfully from nodes to the hub, thus the normalized throughput of UP_k nodes increases as the distance increases.

The relationship of normalized throughput and the number of coexisting WBANs is shown in Fig. 6. The distance from the target WBAN N_1 to its neighbouring WBANs is 2 m in this case. The normalized throughput decreases obviously with the number of coexisting WBANs increases. Multiple coexisting WBANs deteriorate the normalized throughput of higher UP nodes, such as UP_7 and UP_6. The normalized throughput of UP_7 and UP_6 are lower than UP_5 and UP_4 when the number of coexisting WBANs is larger than 4. This is owing to the more accompanying interference with increasing number of WBANs.

B. Average Access Delay

The average access delay will decrease with the increasing distance between adjacent WBANs. Fig. 7 shows that the interference nodes have a big impact on high UPs nodes. The UP_7 nodes with no interference take about less than fifty percent of the time cost when the distance between two adjacent WBANs is zero. The lower UPs changes little on the delay while the distance changes. The UP_0 changes from 62.99 ms to 60.20 ms and UP_1 changes from 39.8 ms to 37 ms during the number of interfering nodes changing maximum to minimum. The reason is that the lower UP nodes are weak in the contention progress and they have to suffer a long back-off procedure in the collision process at the same time.

The average access delay of UP_k nodes is shown in Fig. 8. We can observe that the delay of UP_k (except UP_7) nodes

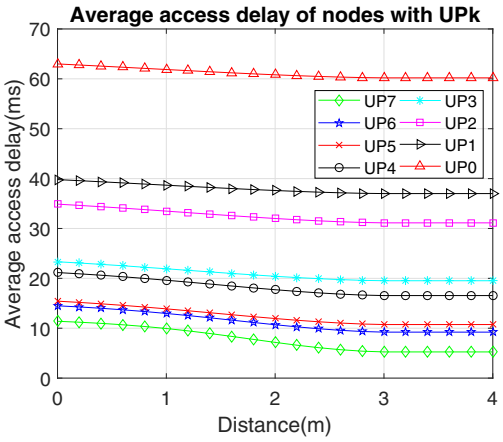

Fig. 7: Average access delay versus the distance between N_1 and N_m.

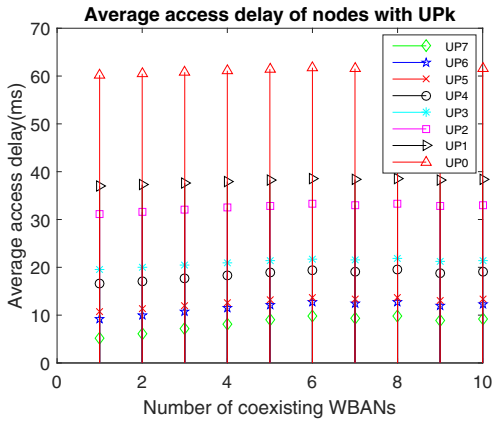

Fig. 8: Average access delay versus the number of coexisting WBANs.

rises slowly with the increasing number of coexisting WBANs. The delay of UP_7 is 5.25 ms when there is no neighbouring WBANs, and the delay rises to 9.23 ms when there are 9 interfering neighbours. The interference heavily affects the timeliness of emergency data transmission. The interference mitigation schemes must be put on the schedule.

VI. Conclusion

In this paper, we have analyzed the dynamic interference generated by varying number of interfering nodes from neighbour WBANs owing to human mobility in multi-WBAN coexisting scenario. The movement of neighbouring WBANs in rectilinear motion and curvilinear motion cases have been investigated. The normalized throughput and average access delay under different interference conditions have been derived in tractable expressions, which are useful in network configuration and interference mitigation. In the future, we will focus on the interference mitigation schemes in coexisting mobile WBANs.

Acknowledgment

This work was supported by the National Natural Science Foundation of China under Grant No. 61571350, Key Research and Development Program of Shaanxi (Contract No. 2017KW-004, 2017ZDXM-GY-022), and the 111 Project (B08038).

References

[1] R. Chavez-Santiago, K. Sayrafian-Pour, A. Khaleghi, K. Takizawa, J. Wang, I. Balasingham, and H.-B. Li, "Propagation models for IEEE 802.15. 6 standardization of implant communication in body area networks," *IEEE Commun. Mag.*, vol. 51, no. 8, pp. 80–87, 2013.

[2] A. Boulis, D. Smith, D. Miniutti, and L. Libman, "Challenges in body area networks for healthcare: the MAC," *IEEE Commu. Mag.*, vol. 50, no. 5, pp. 100–106, 2012.

[3] A. Al-Fuqaha, M. Guizani, M. Mohammadi, M. Aledhari, and M. Ayyash, "Internet of things: A survey on enabling technologies, protocols, and applications," *IEEE Commun. Surveys Tuts.*, vol. 17, no. 4, pp. 2347–2376, 2015.

[4] Q. Ye and W. Zhuang, "Distributed and adaptive medium access control for internet-of-things-enabled mobile networks," *IEEE Internet Things J.*, vol. 4, no. 2, pp. 446–460, 2017.

[5] A. Samanta and S. Misra, "Energy-efficient and distributed network management cost minimization in opportunistic wireless body area networks," *IEEE Trans. Mobile Comput.*, vol. PP, no. 99, pp. 1–14, 2017.

[6] X. Wu, Y. I. Nechayev, C. C. Constantinou, and P. S. Hall, "Interuser interference in adjacent wireless body area networks," *IEEE Trans. Antennas Propag.*, vol. 63, no. 10, pp. 4496–4504, 2015.

[7] T. T. T. Le and S. Moh, "Interference mitigation schemes for wireless body area sensor networks: A comparative survey," *Sensors*, vol. 15, no. 6, pp. 13 805–13 838, 2015.

[8] X. Wang and L. Cai, "Interference analysis of co-existing wireless body area networks," in *Proc. of IEEE GLOBECOM*. Houston, TX, USA, Dec. 2011, pp. 1–5.

[9] W. Sun, Y. Ge, Z. Zhang, and W.-C. Wong, "An analysis framework for interuser interference in IEEE 802.15. 6 body sensor networks: A stochastic geometry approach," *IEEE Trans. Veh. Technol.*, vol. 65, no. 10, pp. 8567–8577, 2016.

[10] Z. Zhang, H. Wang, C. Wang, and H. Fang, "Interference mitigation for cyber-physical wireless body area network system using social networks," *IEEE Trans. on emerging topics in computing*, vol. 1, no. 1, pp. 121–132, 2013.

[11] S. Cheng, C. Huang, and C. C. Tu, "Racoon: a multiuser qos design for mobile wireless body area networks." *J. Med. Syst.*, vol. 35, no. 5, pp. 1277–1287, 2011.

[12] S. Kim, S. Kim, J. W. Kim, and D. S. Eom, "Flexible beacon scheduling scheme for interference mitigation in body sensor networks," in *Proc. of IEEE SECON*. Seoul, Korea (South), Jun.2012, pp. 157–164.

[13] I. S. Association, "IEEE standard for local and metropolitan area networks-part 15.6: wireless body area networks," *IEEE Std for Information Technol., IEEE*, vol. 802, no. 6, pp. 1–271, 2012.

[14] S. Rashwand, J. Mišić, and V. B. Mišić, "Analysis of CSMA/CA mechanism of IEEE 802.15. 6 under non-saturation regime," *IEEE Trans. Parallel Distrib. Syst.*, vol. 27, no. 5, pp. 1279–1288, 2016.